

# Stochastic gravitational-wave background searches and constraints on neutron-star ellipticity

Federico De Lillo,<sup>\*</sup> Jishnu Suresh,<sup>†</sup> Andrew L. Miller<sup>‡</sup>

*Centre for Cosmology, Particle Physics and Phenomenology (CP<sup>3</sup>),  
Université catholique de Louvain, Louvain-la-Neuve, B-1348, Belgium*

Accepted XXX. Received YYY; in original form ZZZ

## ABSTRACT

Rotating neutron stars (NSs) are promising sources of gravitational waves (GWs) in the frequency band of ground-based detectors. They are expected to emit quasi-monochromatic, long-duration GW signals, called continuous waves (CWs), due to their deviations from spherical symmetry. The degree of such deformations, and hence the information about the internal structure of a NS, is encoded in a dimensionless parameter  $\varepsilon$  called ellipticity. Searches for CW signals from isolated Galactic NSs have shown to be sensitive to ellipticities as low as  $\varepsilon \sim O(10^{-9})$ . These searches are optimal for detecting and characterising GWs from individual NSs, but they are not designed to measure the properties of NSs as population, such as the average ellipticity  $\varepsilon_{\text{av}}$ . These ensemble properties can be determined by the measurement of the stochastic gravitational-wave background (SGWB) arising from the superposition of GW signals from individually-undetectable NSs. In this work, we perform a cross-correlation search for such a SGWB using the data from the first three observation runs of Advanced LIGO and Virgo. Finding no evidence for a SGWB signal, we set upper limits on the dimensionless energy density parameter  $\Omega_{\text{gw}}(f)$ . Using these results, we also constrain the average ellipticity of Galactic NSs and five NS “hotspots”, as a function of the number of NSs emitting GWs within the frequency band of the search  $N_{\text{band}}$ . We find  $\varepsilon_{\text{av}} \lesssim 1.8 \times 10^{-8}$ , with  $N_{\text{band}} = 1.6 \times 10^7$ , for Galactic NSs, and  $\varepsilon_{\text{av}} \lesssim [3.5 - 11.8] \times 10^{-7}$ , with  $N_{\text{band}} = 1.6 \times 10^{10}$ , for NS hotspots.

**Key words:** gravitational waves – neutron stars

## 1 INTRODUCTION

Isolated, rotating, non axi-symmetric neutron stars, with a rotational period of the order of milliseconds, are promising sources of GWs for ground-based GW detectors, such Advanced LIGO (Aasi et al. 2015), Advanced Virgo (Acernese et al. 2015), and KAGRA (Akutsu et al. 2021). Such objects would emit GWs due to deformations on their surfaces, i.e. “mountains” (Jones & Andersson 2002), due to a strong internal magnetic field (Osborne & Jones 2020), accretion from a companion (Ushomirsky et al. 2000; Meadors et al. 2016; Haskell & Patruno 2017; Singh et al. 2020) or toroidal perturbations throughout the star, i.e. r-modes (Owen et al. 1998; Mytidis et al. 2015, 2019). The size of these deformations, and the rate at which neutron stars accrete matter, are estimated to be small (Lasky 2015); thus, these processes would emit GWs at an almost fixed frequency by extracting rotational energy from the neutron star on a timescale much longer than the observation time of GW detectors (Maggiore 2007). These are called continuous waves: quasi-monochromatic, long-duration GWs. Methods to search for CWs have been developed (Riles 2017; Sieniawska & Bejger 2019; Tenorio et al. 2021; Juliana 2022) and are currently used for all-sky (Abbott et al. 2021h), directed (Aasi et al. 2013; Dergachev et al. 2019; Piccinni et al. 2020; Abbott et al.

2021j), targeted (Abbott et al. 2021a,i, 2020, 2021b) and post-merger remnant searches (Abbott et al. 2019, 2017; Oliver et al. 2019; Sun & Melatos 2019; Miller et al. 2018, 2019; Banagiri et al. 2019). CW methods have even been adapted to search for particle dark matter (Pierce et al. 2018; Guo et al. 2019; Miller et al. 2021c; Abbott et al. 2021c), boson clouds around black holes (Palomba et al. 2019; Isi et al. 2019; Sun et al. 2020) and primordial black hole binaries (Miller et al. 2021a,b), all of which underscore the broad scope of CW physics. However, no method or search mentioned so far for neutron stars or dark matter, no matter how exotic, has allowed us to probe bulk properties of isolated neutron stars.

Though no CW has been detected yet, each type of CW search has shown promising results. Targeted searches continue to surpass the GW-amplitude spin-down limit, which assumes that all of the rotational energy lost by NSs as they spin-down is through GW radiation (Abbott et al. 2021a, 2020, 2021i). Additionally, all-sky and directed searches probe smaller and smaller deformations at galactic-centre distances (Abbott et al. 2021d, 2022). The improved sensitivity of these searches over time brings us closer and closer to being able to make a detection of a CW from an isolated NS. Moreover, once we enter the detection era, GWs could be used as a novel messenger to identify new nearby NSs, an alternative to current searches for pulsars in electromagnetic (EM) data, whose average discovery rate is  $\approx 50 \text{ yr}^{-1}$ . However, assuming the Galactic supernovae rate to be  $10^{-2} \text{ yr}^{-1}$  (Diehl et al. 2006) and the age of the Milky Way to be  $10^{10}$  yrs, there are roughly  $\sim 10^8$  NSs (Reed et al.

<sup>\*</sup> E-mail: federico.delillo@uclouvain.be

<sup>†</sup> E-mail: jishnu.suresh@uclouvain.be

<sup>‡</sup> E-mail: andrew.miller@uclouvain.be

2021) in our Galaxy alone. This large number of NSs implies that, even in the detection era, assuming a CW discovery rate of the same order or even ten times greater than the average electromagnetic one, we would still need centuries to individually detect the majority of the NSs and characterise the Galactic NS population properties. It is also not clear how many isolated NSs would need to be individually detected to make population-based statements. In addition, current CW searches are not yet designed to provide information on NS ensemble properties, even though methods have been developed to combine results from targeted searches for a few hundreds of known pulsars (Fan et al. 2016; Pitkin et al. 2018; Buono et al. 2021). Nonetheless, this is just a small fraction of the larger population considered here, and suggests the need for an alternative strategy to determine such properties that do not rely on measuring GWs from individual NSs.

We attempt to address this problem by searching for an astrophysical stochastic gravitational-wave background (SGWB) (Abbott et al. 2018; Rosado 2011; Marassi et al. 2011; Zhu et al. 2011, 2013; Dvorkin et al. 2016; Dhurandhar et al. 2011; Hughes 2014; Cusin et al. 2019; Bar-Kana 1994; Cook & Sorbo 2012; Regimbau 2011; Inayoshi et al. 2021; Watanabe & Komatsu 2006; Kamionkowski et al. 1994; Kosowsky et al. 1992; Turner 1997) from the superposition of weak GW signals from individually-undetectable pulsars, which could already be observed by current detectors (Talukder et al. 2014). Its detection and characterisation would provide constraints that are independent and complementary to those inferred from CW (and EM) searches for individual NSs. Moreover, it would give insight into ensemble properties of NSs, by identifying certain traits (e.g. the mean value) of the statistical distributions of the parameters (e.g. the ellipticity), which characterise the population of interest, at once.

In this work, we consider the Galactic-NS population and the NS populations of five "hotspots", i.e. patches of the sky that are expected to have a high number of NSs (Dhurandhar et al. 2011; Okada et al. 2012), as potential candidates for our search. For each of these cases, we use cross-correlation (Allen & Ottewill 1997; Romano & Cornish 2017; Allen & Romano 1999) methods to search for a SGWB. Cross-correlation allows us to search for a common signal in multiple data streams simultaneously and disentangle it from instrumental noise. From these measurements, we could measure the number of Galactic NSs emitting in a given frequency band, and the average ellipticity of that population  $\varepsilon_{\text{av}}$ . However, the search employed in this work finds no evidence of such a background; therefore, we set limits on the SGWB properties and then convert them into constraints on the average ellipticity of each population as a function of the number of NSs emitting GWs within the frequency band of the search.

The paper is organised as follows. In Section 2, we describe the SGWB signal from isolated, rotating NSs, and model the NS population as a function of frequency using the known pulsars from the ATNF catalogue (Manchester et al. 2005). In Section 3, we present the cross-correlation techniques and show how to estimate the average ellipticity of a population of pulsars from the results of our search for a SGWB signal. Then, in Section 4, we illustrate the results of the searches for a SGWB from NSs when using the data from the first three observation runs of Advanced LIGO and Virgo over the population of Galactic NSs, and the NSs of the five hotspots: Virgo, Fornax, Antlia, Centaurus, and Hydra galaxies clusters, which contain thousands of galaxies and are assumed to have roughly 1000 times more NSs than our Galaxy. In addition to that, we express the results as limits on the average ellipticities of the considered populations. Finally, in Section 5, we summarise and discuss the implications of

our results in terms of possible synergies between CW searches and SGWB ones, and future extensions to this work.

## 2 MODELLING THE SOURCE

The strain amplitude of a GW emitted from an isolated, rotating, non-axi-symmetric NS at a distance  $d$  from Earth, with a moment of inertia along the z-axis  $I_{zz}$ , and an ellipticity  $\varepsilon \equiv \frac{I_{xx}-I_{yy}}{I_{zz}}$ , in the quadrupole approximation (Maggiore 2007), is given as

$$h_0(f) = \frac{4\pi^2 G \varepsilon I_{zz}}{c^4 d} f^2, \quad (1)$$

where  $G$  is Newton's gravitational constant,  $c$  is the speed of light, and  $f$  is the frequency of the emitted GW, which is twice the rotational frequency of the NS. Using equation (1), it is possible to show that (see appendix A) an ensemble of pulsars, whose contributions are summed incoherently, generates a GW power spectral density  $H(f)$

$$H(f) = \frac{32\pi^4 G^2 \langle \varepsilon^2 \rangle_{\text{NS}} \langle I_{zz}^2 \rangle_{\text{NS}}}{5c^8} \left\langle \frac{1}{d^2} \right\rangle_{\text{NS}} f^4 N(f), \quad (2)$$

where the angular brackets  $\langle \dots \rangle_{\text{NS}}$  denote the ensemble average over the NS population, and  $N(f)$  is the number of NSs emitting GWs between frequencies  $f$  and  $f + df$ . To completely determine the frequency dependence of this stochastic signal, we rewrite  $N(f)$  as

$$N(f) = N_0 \Phi(f), \quad (3)$$

where  $N_0$  is the number of NSs in a given ensemble, and  $\Phi(f)$  is the corresponding probability distribution function (PDF) of the NSs frequencies, defined such that

$$N_0 \int_{-\infty}^{\infty} \Phi(f) df = N_0. \quad (4)$$

We consider  $N_0 \sim 10^8$  when studying the SGWB from Galactic NS, and  $N_0 \sim 10^{11}$  when analysing the NS hotspots. To model  $\Phi(f)$ , we employ an observation-driven approach (Reed et al. 2021), and use information about known pulsars available in the ATNF catalogue (Manchester et al. 2005). We start from the ( $\log_{10}$ -) frequency distribution of the  $\approx 3000$  pulsars available in the catalogue and obtain the frequency distribution PDF through a Gaussian kernel-density-estimator (KDE) (Virtanen et al. 2020). The resulting  $\Phi(f)$  is shown in Figure 1. Even though the number of NSs used to construct  $\Phi(f)$  is just a tiny fraction of the pulsars within our Galaxy and clusters of galaxies, the frequency distribution is expected to not be significantly biased by selection effects (Lorimer 2008; Lorimer et al. 2019) for millisecond pulsars. Moreover, this distribution is consistent with those obtained from population synthesis models (Story et al. 2007; Talukder et al. 2014). From Figure 1, it is interesting to note that  $\Phi(f)$  displays a secondary peak at 526 Hz, which incidentally falls within the frequency band to which ground-based GW detectors are sensitive. The unnormalised spectral shape  $H(f)$  corresponding to the computed  $\Phi(f)$  is shown in Figure 2. In this spectrum, due to the dominant contribution from the  $f^4$  term in equation (2), the peak is shifted to a higher frequency (1688 Hz).

Given  $\Phi(f)$  and  $N_0$ , we define  $N_{\text{band}}$  as the "in-band" NS number, which quantifies the number of NSs between a lower frequency  $f_{\text{min}}$  and a higher frequency  $f_{\text{max}}$ . Thus, we can write  $N_{\text{band}}$  for the SGWB search described in this work as

$$N_{\text{band}} = N_0 \int_{f_{\text{min}}}^{f_{\text{max}}} \Phi(f) df = N_0 \int_{20\text{Hz}}^{1726\text{Hz}} \Phi(f) df \approx 0.16 N_0, \quad (5)$$

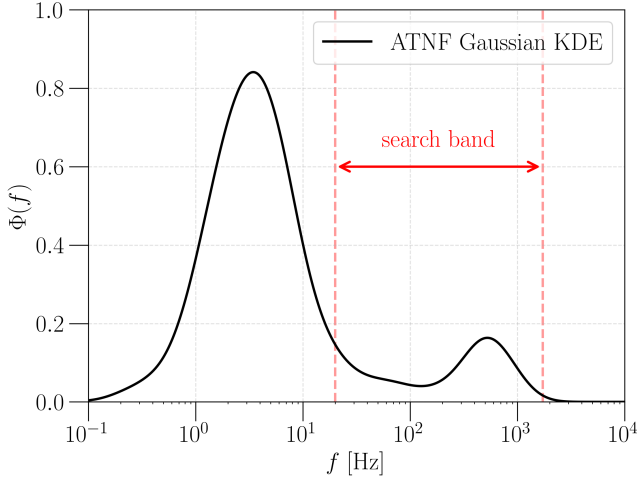


**Figure 1.** The frequency distribution of the PDF  $\Phi(f)$ , generated from the ATNF catalogue data. The red-dashed vertical lines show the frequency band 20-1726 Hz used in our search.

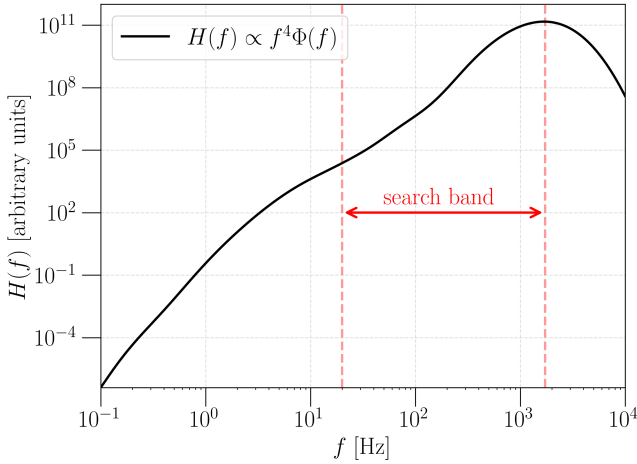


**Figure 2.** Unnormalised spectral shape  $H(f)$  as a function of frequency, assuming  $\Phi(f)$  derived from a Gaussian KDE using data from the ATNF catalogue. The red-dashed vertical lines show the frequency range that we analyse in our search.

where the 20-1726 Hz denotes our chosen frequency band for this search<sup>1</sup>. We analyse this frequency band because current GW detectors are most sensitive to signals arising between 20-1726 Hz (Thrane & Romano 2013), and it contains the GW emission-band of millisecond pulsars. We also note that only 16% of NSs emit GWs in our chosen frequency band. However, this fraction translates into  $\sim 10^7$  and  $\sim 10^{10}$  in-band NSs in the galactic and hotspot cases, respectively, all emitting CWs, whose superposition would give rise to a continuous, Gaussian (due to the central limit theorem) SGWB. In this study, we rely on the spectral shape given in equation (2) to describe the SGWB from NS populations. By assuming a canonical value for  $\langle I_{zz}^2 \rangle_{\text{NS}}^{1/2} = 1.1 \times 10^{38} \text{ kg m}^2$ , and a fiducial value  $\langle 1/d^2 \rangle_{\text{NS}}^{-1/2}$

<sup>1</sup> The frequency range used in this analysis is consistent with the previous stochastic searches (Abbott 2021a,b)

for each population, we can translate the measurement of a SGWB into constraints on  $\varepsilon_{\text{av}}$  as a function of  $N_{\text{band}}$ . It is worth noting here that, along with equation (2), it would be interesting to consider the angular distribution of pulsars to characterise the stochastic GW signal. This is because, from current observations, the Galactic NS angular distribution is likely to be anisotropic, i.e. peaked towards the galactic plane (Lorimer 2012), and the hotspots are localised in specific sky regions. However, in this work, we treat the SGWB from Galactic NSs as isotropic and consider the average power strain of the hotspots. Considering all the anisotropies in the SGWB sky would require us to employ the matched-filtering “ $\lambda$ -statistic” proposed in Talukder et al. (2011), and produce a template bank, which is out of the scope of the present work.

### 3 SEARCH METHODS

Searches for a SGWB typically characterise the fractional energy density  $\Omega_{\text{GW}}$  (Allen & Romano 1999; Allen & Ottewill 1997; Cornish & Romano 2015; Mingarelli et al. 2019), which is defined as the ratio between  $\rho_{\text{GW}}$ , the energy density from all GWs in the Universe, and  $\rho_c \equiv \frac{3H_0^2 c^2}{8\pi G}$ , the critical density needed to have a flat Universe. Here,  $H_0 = 67.9 \text{ km s}^{-1} \text{ Mpc}^{-1}$  (Ade et al. 2016) is Hubble’s parameter today.  $\Omega_{\text{GW}}$  receives contributions from GWs at all frequencies and it is natural to study its frequency spectrum

$$\Omega_{\text{gw}}(f) = \frac{f}{\rho_c} \frac{d\rho_{\text{gw}}(f)}{df}, \quad (6)$$

which is related to  $H(f)$  by

$$\Omega_{\text{gw}}(f) = \frac{2\pi^2}{3H_0^2} f^3 H(f). \quad (7)$$

Since we are performing a search that assumes GW sources to be isotropically distributed in the sky, equation (6) fully characterises the SGWB.

#### 3.1 The cross-correlation search for an isotropic SGWB

As illustrated in the above discussion, we first perform a search for a Gaussian, stationary, unpolarised, isotropic SGWB. We use GW strain data from the LIGO-Hanford (H), LIGO-Livingston (L), and Virgo (V) detectors, and follow the search procedures in Abbott (2021a). For each detector pair, called a “baseline  $IJ$ ” ( $I, J = H, L, V$ ), we divide the time-series output  $s_I(t)$  in segments of duration  $\tau$ , labelled by  $t$ , take their Fourier-transforms  $\tilde{s}_I(t; f)$ , and calculate a cross-correlation statistic in each segment. Thus, we can define the cross-correlation estimator at every frequency, usually referred as the “narrowband estimator”, as (Romano & Cornish 2017)

$$\hat{C}_{IJ}(t; f) = \frac{2}{\tau} \frac{\Re[\tilde{s}_I^*(t; f) \tilde{s}_J(t; f)]}{\gamma_{IJ}(f) S_0(f)}, \quad (8)$$

where  $S_0(f) = (3H_0^2)/(10\pi^2 f^3)$ , and  $\gamma_{IJ}(f)$  is the normalised isotropic overlap reduction function (ORF) (Allen & Romano 1999; Christensen 1992; Flanagan 1993) of the baseline  $IJ$ . The ORF quantifies the reduction in sensitivity due to the geometry of baseline and its response to the GW signal. The normalisation of the ORF is done in such a way that  $\langle \hat{C}_{IJ}(t; f) \rangle = \Omega_{\text{gw}}(f)$  in the absence of correlated noise. The variance associated with the above estimator, in the small signal limit, can be expressed as

$$\sigma_{IJ}^2(t; f) \approx \frac{1}{2\tau \Delta f} \frac{P_I(t; f) P_J(t; f)}{\gamma_{IJ}^2(f) S_0^2(t; f)}, \quad (9)$$

where  $P_I(t; f)$  is the one-sided power spectral density (PSD) in a detector, while  $\Delta f$  denotes the frequency resolution.

Starting from the narrowband estimator  $\hat{C}_{IJ}(t; f)$ , we can build a broadband optimal estimator  $\hat{C}_{IJ}$  by combining the cross-correlation spectra from different frequencies with appropriate weight factors. This optimal estimator and the associated uncertainty can be expressed as

$$\hat{C}_{IJ} = \frac{\sum_{k,t} w(f_k) \hat{C}_{IJ}(t; f_k) \sigma_{IJ}^{-2}(t; f_k)}{\sum_k w^2(f_k) \sigma_{IJ}^{-2}(t; f_k)}, \quad (10)$$

$$\sigma_{IJ}^{-2} = \sum_{k,t} w^2(f_k) \sigma_{IJ}^{-2}(t; f_k), \quad (11)$$

where  $f_k$  is a set of discrete frequencies. The weights  $w(f)$  can be derived for a generic  $\Omega_{\text{gw}}(f)$  following an optimal filtering approach (Romano & Cornish 2017)

$$w(f) = \frac{\Omega_{\text{gw}}(f)}{\Omega_{\text{gw}}(f_{\text{ref}})}, \quad (12)$$

where  $f_{\text{ref}}$  is an arbitrary reference frequency, fixed at  $f_{\text{ref}} = 25$  Hz in this analysis to be consistent with (Abbott 2021a). After calculating the cross-correlation statistics for each pair of detectors, we can combine the individual broadband estimators from independent baselines (HL, HV, LV) as well as past observing runs (O1-HL, O2-HL) to obtain the final estimator  $\hat{C}$  and its uncertainty:

$$\hat{C} = \frac{\sum_{IJ} \hat{C}^{IJ} \sigma_{IJ}^{-2}}{\sum_{IJ} \sigma_{IJ}^{-2}} \quad (13)$$

$$\sigma^{-2} = \sum_{IJ} \sigma_{IJ}^{-2}. \quad (14)$$

Now, we can recast  $\Omega(f)$  in equation (7) (by means of equation (2)) and rearranging the terms) in the following form:

$$\Omega_{\text{gw}}(f) = \Omega_{\text{ref}} \left( \frac{f}{f_{\text{ref}}} \right)^7 \frac{\Phi(f)}{\Phi(f_{\text{ref}})}. \quad (15)$$

Finally, after applying the relevant data quality cuts (Abbott et al. 2021e; Abbott 2021a), and vetoing all outliers found in our search, we can use the estimators presented in equation (13) to set upper limits on  $\Omega_{\text{ref}}$  through a Bayesian analysis for the model of interest. To do that, we employ the likelihood

$$p(\hat{C}(f_k) | \Omega(f_k)) = \frac{1}{\sqrt{2\pi}\sigma(f_k)} \exp \left[ -\frac{(\hat{C}(f_k) - \Omega(f_k))^2}{2\sigma^2(f_k)} \right], \quad (16)$$

where  $\hat{C}(f_k)$  is assumed to be Gaussian distributed in absence of a signal (Romano & Cornish 2017) and  $\Omega(f_k)$  is the model for the SGWB in equation (15). Moreover, we can also use the estimator for  $\Omega_{\text{ref}}$  as a starting point to obtain a constraint on  $\varepsilon_{\text{av}}$  of a NS population as a function of  $N_{\text{band}}$ , which will be discussed next.

### 3.2 Constraining the ellipticity of a NS population

Here, we show how to translate the results of the above-presented analysis to build an estimator for the average ellipticity of a NS population. We recall from section 2 that we are using fiducial values for  $\langle I_{zz}^2 \rangle_{\text{NS}}^{1/2}$  and  $\langle 1/d^2 \rangle_{\text{NS}}^{-1/2}$ , while  $\varepsilon_{\text{av}}$  and  $N_{\text{band}}$  are left as free parameters for the time being.

Considering equation (2), along with the frequency range of interest, we can rewrite equation (7) as

$$\Omega(f) = \frac{64\pi^6 G^2 \langle \varepsilon^2 \rangle_{\text{NS}} \langle I_{zz}^2 \rangle_{\text{NS}}}{3H_0^2 5c^8} \left\langle \frac{1}{d^2} \right\rangle_{\text{NS}} f^7 N_{\text{band}} \Phi(f). \quad (17)$$

Then, by combining the above equation with equations 12 and 15, we obtain

$$\Omega(f) = \left( \frac{f}{f_{\text{ref}}} \right)^7 \frac{\Phi(f)}{\Phi(f_{\text{ref}})} \xi \langle \varepsilon^2 \rangle_{\text{NS}} = w(f) \xi \langle \varepsilon^2 \rangle_{\text{NS}}, \quad (18)$$

where we have introduced  $\xi = \xi(N_{\text{band}}) \equiv \Omega_{\text{ref}} / \langle \varepsilon^2 \rangle_{\text{NS}}$ , which is just a proportionality constant, once  $N_{\text{band}}$  is fixed. Within this framework, using equation (8), the above equation can be recast in terms of different narrowband estimators:

$$\left( \widehat{\varepsilon^2} \right)_{\text{av}}(f_k) = \frac{1}{\xi} \frac{\hat{C}_{IJ}(f_k)}{w(f_k)} \equiv \frac{\hat{\Omega}_{\text{ref}}(f_k)}{\xi}, \quad (19)$$

where  $\hat{\Omega}_{\text{ref}}(f_k)$  is the narrowband estimator of  $\Omega_{\text{ref}}$ , while  $\left( \widehat{\varepsilon^2} \right)_{\text{av}}(f_k)$  is the narrowband estimator of the average squared ellipticity  $\langle \varepsilon^2 \rangle_{\text{NS}}$  of the NS population<sup>2</sup>.

Starting from the above estimator, we can derive the relationship between  $\left( \widehat{\varepsilon^2} \right)_{\text{av}}(f_k)$  and the average ellipticity of the NS population along with its estimator. This can be done by writing the expectation value of  $\left( \widehat{\varepsilon^2} \right)_{\text{av}}(f_k)$ :

$$\left\langle \left( \widehat{\varepsilon^2} \right)_{\text{av}}(f_k) \right\rangle = \left\langle \varepsilon^2(f_k) \right\rangle_{\text{NS}} \equiv \varepsilon_{\text{av}}^2(f_k) + \sigma_{\varepsilon}^2(f_k), \quad (20)$$

where  $\varepsilon_{\text{av}}(f_k) \equiv \langle \varepsilon(f_k) \rangle_{\text{NS}}$  is the mean value of the ellipticity, while  $\sigma_{\varepsilon}^2(f_k)$  is the intrinsic variance of the ellipticity distribution. Then, from equation (20), we can define the biased estimator of the average ellipticity

$$\hat{\varepsilon}_{\text{av}}(f_k) \equiv \sqrt{\left( \widehat{\varepsilon^2} \right)_{\text{av}}(f_k)}. \quad (21)$$

The bias introduced from the non-zero variance of the ellipticity distribution should be small, since the physical ellipticity is a positive definite quantity. Thus, one can assume  $\sigma_{\varepsilon}(f_k) \lesssim \varepsilon_{\text{av}}(f_k)$  and ignore the variance in equation (20). This choice translates into more conservative constraints derived from  $\hat{\varepsilon}(f_k)$ <sup>3</sup>. Possible ways to account for the bias, as in the case of a detection of a SGWB from a NS population, would be to estimate  $\sigma_{\varepsilon}^2(f_k)$  from the measurements of individual NSs (such as the ones detected with CW/EM techniques) from theoretical models of the population.

Given the estimator  $\hat{\varepsilon}_{\text{av}}(f_k)$ , we can derive the associated uncertainty  $\sigma_{\hat{\varepsilon}}(f_k)$  from the likelihood function  $p_{\varepsilon}(\hat{\varepsilon}_{\text{av}}(f_k) | \varepsilon_{\text{av}}(f_k))$ . To obtain this likelihood, we use equations (18), (19), and (21) to express  $\Omega(f_k)$  and  $\hat{C}(f_k)$  as a function of  $\varepsilon_{\text{av}}(f_k)$  and  $\hat{\varepsilon}_{\text{av}}(f_k)$ , and we perform a change of variables in equation (16). Following this prescription, we obtain the following likelihood function for  $\hat{\varepsilon}_{\text{av}}(f_k)$ , which is no longer a Gaussian:

$$p_{\varepsilon}(\hat{\varepsilon}_{\text{av}}(f_k) | \varepsilon_{\text{av}}(f_k)) = \sqrt{\frac{8}{\pi}} \frac{\varepsilon_{\text{av}}(f_k) \xi}{\sigma_{\hat{\Omega}}(f_k)} \exp \left[ -\frac{(\hat{\varepsilon}_{\text{av}}^2(f_k) - \varepsilon_{\text{av}}^2(f_k))^2 \xi^2}{2\sigma_{\hat{\Omega}}^2(f_k)} \right], \quad (22)$$

where  $\sigma_{\hat{\Omega}}(f_k)$  is the error corresponding to  $\hat{\Omega}_{\text{ref}}(f_k)$ . By applying the definition of variance to the above distribution, in the limit  $\hat{\varepsilon}_{\text{av}}(f_k) \ll 1$ , we arrive at:

$$\sigma_{\hat{\varepsilon}}^2(f_k) |_{\hat{\varepsilon} \ll 1} \approx \left[ \sqrt{\frac{2}{\pi}} - \frac{2^{3/2} \pi}{\Gamma^2(\frac{1}{4})} \right] \frac{\sigma_{\hat{\Omega}}(f_k)}{\xi} \approx 0.12 \frac{\sigma_{\hat{\Omega}}(f_k)}{\xi}. \quad (23)$$

<sup>2</sup> The frequencies  $f_k$  in equation (19) must be interpreted as labels and not as functional dependence.

<sup>3</sup> A non-zero  $\sigma_{\varepsilon}^2(f_k)$  will increase the intensity of a stochastic signal at a fixed  $\varepsilon_{\text{av}}(f_k)$ , making its detection easier.

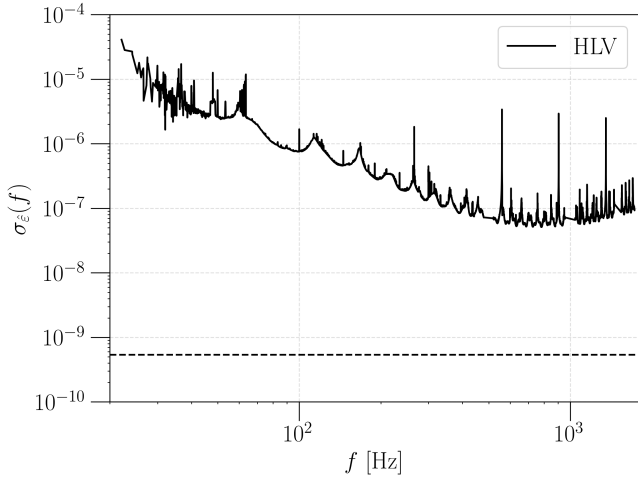


**Figure 3.** Plot of the  $1\sigma$  sensitivity to the average ellipticity of Galactic NSs. The solid curve shows the uncertainty  $\sigma_{\epsilon}(f_k)$  associated to the narrowband estimators, while the dashed one is the broadband value of  $\sigma_{\text{opt}}$ . The improvement of the search sensitivity by combining the narrowband estimators ranges between two and four orders of magnitude. The plot assumes  $N_{\text{band}} = 1.6 \times 10^7$ ,  $\langle 1/d^2 \rangle_{\text{NS}}^{-1/2} = 6$  kpc, and  $\langle I_{zz}^2 \rangle_{\text{NS}}^{1/2} = 10^{38}$  kg m<sup>2</sup>.

The derivation and the expression of  $\sigma_{\hat{\epsilon}}^2(f_k)$  in the general case  $\hat{\epsilon}_{\text{av}}(f_k) > 0$  are reported in Appendix B.

Finally, assuming the ellipticity to be independent of the frequency, the narrowband estimators  $\hat{\epsilon}_{\text{av}}(f_k)$  can be combined to obtain the optimal broadband estimator  $\hat{\epsilon}_{\text{opt}}$ , with a relative uncertainty  $\sigma_{\text{opt}}$  as

$$\hat{\epsilon}_{\text{opt}} = \frac{\sum_k \hat{\epsilon}_{\text{av}}(f_k) \sigma_{\hat{\epsilon}}^{-2}(f_k)}{\sum_k \sigma_{\hat{\epsilon}}^{-2}(f_k)}, \quad \sigma_{\text{opt}} = \left( \sum_k \sigma_{\hat{\epsilon}}^{-2}(f_k) \right)^{-1/2}. \quad (24)$$

Using equation (17) and plugging it into the above equation, the optimal estimator depends on the number of in-band NSs, which has been considered as a free parameter in the analysis, through the relation  $\hat{\epsilon}_{\text{opt}} \propto N_{\text{band}}^{-1/2}$ . Hence, the upper limits on the average ellipticity  $\epsilon_{\text{av}}$  will also depend on  $N_{\text{band}}$ . In this situation, we could set upper limits on quantities such as  $\epsilon_{\text{av}} N_{\text{band}}^{1/2}$  or  $\epsilon_{\text{av}}^2 N_{\text{band}}$ , which are inherently independent from  $N_{\text{band}}$ . Alternatively, we could evaluate upper limits on  $\epsilon_{\text{av}}$  at a reference value of  $N_{\text{band}}$ , and then map them into the  $N_{\text{band}} - \epsilon_{\text{av}}$  plane. In this paper, we follow the second approach to present constraints on the average ellipticity.

## 4 RESULTS OF THE ANALYSES

We perform this analysis on publicly available data (Abbott et al. 2021g) from the first three observing runs (O1, O2, and O3) of the Advanced LIGO and Virgo detectors. We first search for an isotropic SGWB from Galactic NSs, assuming the model given in equation (15). Using these search results, we also place upper limits on the average ellipticity of the NS population. Secondly, we consider five clusters of galaxies as hotspots of GWs. By associating a specific patch<sup>4</sup> in the sky to each of them, we again set constraints on the

<sup>4</sup> The methodology to build the sky patches and evaluate the associated average background are presented in appendix C, and makes use of the radiometer search (Ballmer 2006; Mitra et al. 2008; Abbott et al. 2007).

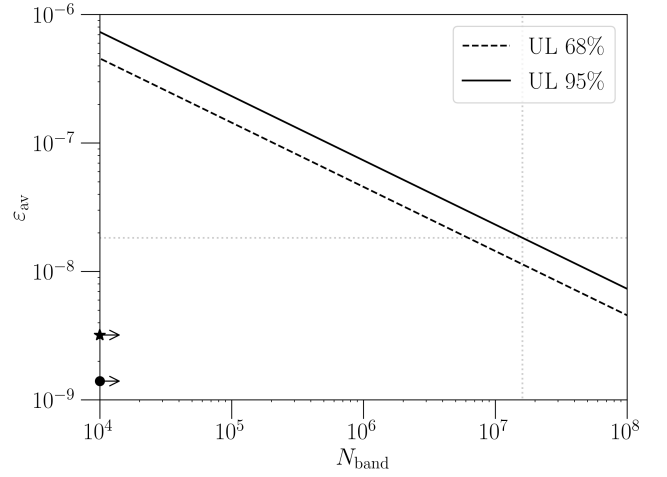


**Figure 4.** 68% (dashed) and 95% (solid) confidence-level Bayesian upper limits in the  $N_{\text{band}} - \epsilon_{\text{av}}$  plane, assuming a log-uniform prior on  $\epsilon_{\text{av}}$ . Here, we have set  $N_{\text{band}}$  to range from  $10^4$  and  $10^8$ . The dotted grey lines identify the 95% upper limit on  $\epsilon_{\text{av}}$  obtained with the pivot value of in-band NSs,  $N_{\text{band}} = 1.6 \times 10^7$ . The star and the circle on the y-axis denote the most recent, lowest upper-limits on a single NS ellipticity (independent of  $N_{\text{band}}$ ), respectively  $\epsilon \lesssim 3.2 \times 10^{-9}$  from targeted (Abbott et al. 2021a) CW searches and  $\epsilon \lesssim 1.4 \times 10^{-9}$  from all-sky (Abbott et al. 2022) ones.

average ellipticity of the NS population starting from the results for the fractional SGWB energy density for each sky patch analysed,  $\Omega_{\text{gw}}^{\text{patch}}(f)$ . These results are given in the following subsections.

### 4.1 Galactic NS results

Since our search for an isotropic SGWB from Galactic isolated NSs did not find any evidence for a signal, we set upper limits on  $\Omega_{\text{ref}}$ . These results are subsequently used to constrain  $\epsilon_{\text{av}}$ , and are listed in table 1. The first four columns from the left contain the results for the SGWB background search. The second column shows the value of the cross-correlation statistic and the associated  $1\sigma$  uncertainty derived from equation (13). The third and fourth columns present the 95% confidence-level Bayesian upper limits for  $\Omega_{\text{ref}}$ . These upper limits are obtained by marginalising the likelihood function given in equation (16) over a uniform (third column) and a log-uniform prior (fourth column) on the strength of the SGWB. It is worth noting that the log-uniform prior seems to be the most natural choice, since  $\Omega_{\text{ref}}$  range is expected to span several orders of magnitude, and is more sensitive to small signals. The log-uniform prior range was chosen to be between  $10^{-18} \leq \Omega_{\text{ref}} \leq 10^{-8}$ . The upper bound is large enough such that there is no posterior support at that value, while the lower bound cannot be zero for this kind of prior. On the other hand, we have also included the result from the uniform prior case, which leads to more conservative upper limits. In both cases, the estimator for  $\Omega_{\text{ref}}$ , as well as the upper limits, are all of  $O(10^{-14})$ . These values are significantly smaller than those for other power-law models for  $\Omega_{\text{gw}}(f)$ , e.g. those reported in Abbott (2021a), since the  $\Omega_{\text{gw}}$  used in this paper is dominated by the  $\sim f^7$  term.

The last two columns in table 1 illustrate the limits we have obtained on the average ellipticity at  $1\sigma$  sensitivity and the corresponding 95% Bayesian upper limits on  $\epsilon_{\text{av}}$ , using the fiducial value  $\langle 1/d^2 \rangle^{-1/2} = 6$  kpc in equation (2). The value of the estimator  $\hat{\epsilon}_{\text{opt}}$  is of  $O(10^{-11})$ , with an associated uncertainty one order of mag-

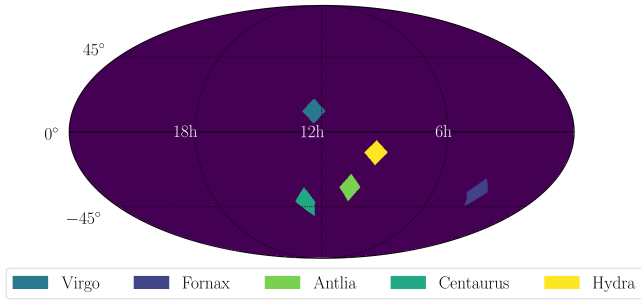


**Figure 5.** The sky-patches associated with the five NS hotspots: Virgo, Fornax, Antlia, Centaurus, and Hydra clusters. Each patch consists of 9 pixels with  $N_{\text{side}} = 16$ : the central one being the one associated with the galaxy cluster, and the eight closest neighbours. The sky map is represented as a Mollweide projection of the sky in ecliptic coordinates.

nitude larger. The improvement in the sensitivity of the search, that comes from combining the estimators over frequencies, is illustrated in figure 3. Here, the relative uncertainties associated to  $\varepsilon_{\text{av}}(f_k)$  and  $\varepsilon_{\text{opt}}$  are plotted as a function of frequency.

On the other hand, the Bayesian upper limit on the average ellipticity  $\varepsilon_{\text{av}}$  has been obtained using the likelihood function in equation (22) by assuming a log-uniform prior in the range  $10^{-12} - 10^{-4}$ . The obtained constraint is of  $\mathcal{O}(10^{-8})$ . As discussed in section 3.2, the constraint holds only for the representative value of  $N_{\text{band}}$  that we have explicitly presented here. However, it can be easily mapped into the  $N_{\text{band}} - \varepsilon_{\text{av}}$  plane for different values of in-band NSs. Considering the range  $N_{\text{band}} \in [10^4 - 10^8]$ , we present the 68% and 95% Bayesian upper limits on the average ellipticity in figure 4. In this figure, the pivot value  $N_{\text{band}} = 1.6 \times 10^7$  is highlighted using a dotted line for an easy comparison. We also report the latest, lowest upper limits on a NS ellipticity from targeted (Abbott et al. 2021a) and all-sky (Abbott et al. 2022) CW searches on the y-axis. It is evident from the figure that the resulting  $\varepsilon_{\text{av}}$ , ranging between  $10^{-8}$  and  $10^{-6}$ , follows the  $\varepsilon_{\text{av}} \propto N_{\text{band}}^{-1/2}$  relation, as anticipated in section 3.2.

## 4.2 Hotspot results

The search results from five NS GW hotspots and the corresponding constraints on their ellipticities are reported in table 2. First, we pixelate the sky by employing the HEALPix (Hierarchical Equal Area isoLatitude Pixelation) pixelisation scheme (Górski et al. 2005; Zonca et al. 2019), with  $N_{\text{side}} = 16$  (3072 pixels, each one with an extension of  $\approx 13.4 \text{ deg}^2$ ). From the right ascension and declination of the hotspot, we identify one pixel and its eight closest neighbours. These collections of pixels will act as a patch in the pixelated sky and are illustrated in figure 5. The signal model for each of the hotspots is similar to the one used in the Galactic NS analysis, except for the number of in-band NS (which in this case is  $N_{\text{band}} = 1.6 \times 10^{10}$ ), and the distance parameter  $\langle 1/d^2 \rangle_{\text{NS}}^{-1/2}$  (values considered are shown in the second column of table 2). For each hotspot, we first estimated the  $\Omega_{\text{gw}}^{\text{patch}}(f)$  using the folded data (Ain et al. 2015; Abbott et al. 2021f) and PyStoch pipeline (Ain et al. 2018), and then followed the method described in section 3.2 to derive constraints on the average ellipticity of the NS populations in each of the hotspots.

Within the above framework, we have derived the optimal estimators and the 95% confidence upper limits related to the average ellipticity of the NS populations of the hotspots. These quantities

are respectively reported in the third and fourth columns of table 2. Because of the absence of any detection, we set upper limits using the same criteria as in the Galactic case. We find that the estimators are of the order of  $10^{-10} - 10^{-9}$ , whereas the upper limits of the average ellipticity are around  $10^{-7} - 10^{-6}$ . Comparing the constraints and the relative hotspots distances, we note that the constraints become less stringent when the source is more distant from Earth. By contrasting the hotspot limits with those from Galactic NSs, we observe that the former are one or two orders of magnitude larger than the latter. This difference could arise from several factors, from the model assumed to the characteristics of the ground-based detectors. From a modelling perspective, based on equations 2 and 17, the difference between these two kinds of NS populations is encoded in the average of the inverse squared distance of the source from the Earth, the number of in-band NS, and the size of the examined region of the sky. The hotspot populations are estimated to have  $10^3$  times more NSs compared to the Galactic population but are also  $10^3$  times more distant from Earth. This means that in light of the model considered and the assumed values, the average ellipticity of the cluster NS population should be  $\approx \sqrt{10^3}$  times the Galactic one, in the naive case where the two SGWB have the same intensity. From the detector perspective, instead, the intrinsic sensitivity of the instrument to the source distance and its position in the sky have an impact. The detector becomes less sensitive the more distant the source of interest is. The sensitivity may get even worse if the source is well localised and spends most of the time in the region of the sky where the detectors have poorly observed modes (Romano & Cornish 2017). Given two populations with different positions and spreads in the sky, analyses of these two areas may lead to less stringent upper limits of one population with respect to another one, even though the properties of the two populations' original signals are the same. This effect can be mitigated by combining data from multiple detectors (pairs) of a detector network, but cannot be completely suppressed, due to the intrinsic geometry of the network and its interaction with the GW signal. Further studies to evaluate the impact of the model and choice and the detector network characteristics in the recovery of the signal will be the subject of future work.

## 5 DISCUSSIONS AND CONCLUSIONS

In this work, we have derived constraints on the average ellipticity of a NS population from the results of a cross-correlation-based search for a SGWB. We have considered two classes of NS populations: those in our Galaxy and those in five extra-galactic clusters, which we call NS hotspots. We have not found compelling evidence of a SGWB signal from any of the considered sources and hence have set upper limits on the intensity of the background by bounding the energy density parameter  $\Omega_{\text{gw}}(f)$ . These results have then been translated to constraints of the NS average ellipticity, obtained to be as low as  $\varepsilon_{\text{av}} \lesssim 1.8 \times 10^{-8}$  with  $N_{\text{band}} = 1.6 \times 10^7$  in the case of Galactic NS and  $\varepsilon_{\text{av}} \lesssim [3.5 - 11.8] \times 10^{-7}$  with  $N_{\text{band}} = 1.6 \times 10^{10}$  for those in galaxy clusters. These constraints obtained using the data from the first three observation runs of Advanced LIGO and Virgo are the first of their kind.

If we consider recent results from CW searches for Galactic NSs, whose lowest limits on NSs ellipticities are  $\varepsilon \lesssim 3.2 \times 10^{-9}$  (for J0636+5129) from targeted searches (Abbott et al. 2021a) and  $\varepsilon \lesssim 1.4 \times 10^{-9}$  (for a NS at 10 pc from Earth and at 2047.5 Hz) from all-sky searches (Abbott et al. 2022), we observe that they are one order of magnitude lower than the values reported here. It is not straightforward to compare these limits, since these analy-

$\Omega(f)$	$\hat{c}^{O1+O2+O3}/(10^{-14})$	$\Omega_{\text{ref}}^{95\%, \text{Uniform}}$	$\Omega_{\text{ref}}^{95\%, \text{Log-uniform}}$	$\Phi(f)$	$N_{\text{band}}$	$\hat{\epsilon}_{\text{opt}}^{O1+O2+O3}/10^{-11}$	$\epsilon_{\text{Log-uniform}}^{95\%}$
$\alpha(f)^7 \Phi(f)$	$0.9 \pm 1.9$	$4.5 \times 10^{-14}$	$2.0 \times 10^{-14}$	ATNF-KDE	$1.6 \times 10^7$	$2.5 \pm 53.5$	$1.8 \times 10^{-8}$

**Table 1.** Results of the isotropic search for a SGWB from an ensemble of Galactic NSs using data from the first three LIGO-Virgo-KAGRA observing runs, and the subsequent constraints on the average ellipticity of the Galactic NS population. The first four columns are the results from our search, in which  $\Omega(f)$ , the cross-correlation statistics, and the upper limits on  $\Omega_{\text{ref}}$ , using a uniform and log-uniform prior, are reported. The last four columns encode information about the Galactic NS population, such as  $\Phi(f)$  and  $N_{\text{band}}$ , the average ellipticity optimal estimator, and the upper limit obtained by assuming a log-uniform prior on  $\epsilon$  between  $10^{-12} - 10^{-4}$ .

Hotspot	$\langle 1/d^2 \rangle_{\text{NS}}^{-1/2}$ (Mpc)	$\hat{\epsilon}_{\text{opt}}^{O1+O2+O3}/10^{-9}$	$\epsilon_{\text{Log-uniform}}^{95\%}/10^{-7}$
Virgo	18	$0.6 \pm 10.6$	3.6
Fornax	19	$0.5 \pm 10.1$	3.5
Antlia	40.7	$1.5 \pm 22.1$	7.6
Centaurus	52.4	$1.4 \pm 27.9$	9.6
Hydra	58.3	$3.8 \pm 34.2$	11.8

**Table 2.** Relevant parameters and results of searches for NSs in hotspots. For each cluster of galaxies, a fiducial value of  $\langle 1/d^2 \rangle_{\text{NS}}^{-1/2}$  (second column), the broadband estimator  $\hat{\epsilon}_{\text{opt}}$  (third column), and the 95% confidence level Bayesian upper limits on the average ellipticity of the population (fourth column) are reported. The upper limits have been obtained by assuming a log-uniform prior between  $10^{-12} - 10^{-4}$  over the ellipticities.

ses constrain different properties of NSs. Targeted CW searches are more sensitive to individual NS properties, such as the ellipticity, but must obtain their limits only based on known pulsars. Moreover, all-sky searches have proven to be computationally expensive (order of months to run), and can only search in certain parts of the parameter space semi-coherently, which limits their sensitivities to ellipticities of  $\mathcal{O}(10^{-7})$  and  $\mathcal{O}(10^{-5})$  at  $\mathcal{O}(1)$  kpc at high and low frequencies, respectively (Abbott et al. 2022). Instead, searches for SGWB have become computationally efficient and faster (order of days to run) (Abbott 2021a,b; Ain et al. 2015, 2018; Suresh et al. 2021), but their constraining power is weaker compared to targeted CW searches. In addition to that, they have the advantage (once the results are available) of instantaneously identifying the features of an ensemble of known or unknown NSs, which would otherwise require decades/centuries to be determined through individual NS discoveries. Because SGWB and CW searches attempt to answer different physical questions, they can work in synergy. Using the methods of the former, it would be possible to perform rapid, blind all-sky searches for NS signals and transmit the coordinates of possible outliers as inputs of the latter, for a more refined and sensitive search.

In this work, we have restricted ourselves to constrain the average ellipticity of a NS population, given the number of in-band NSs. We have assumed values for the average squared moment of inertia and the average square inverse distance of the population. We could gain even more information about NS populations by treating these quantities as free parameters. Additionally, we could estimate and set constraints on these quantities through a full Bayesian search, in which priors could be derived from population synthesis simulations. These simulations could also be used to model the NS frequency and angular distributions, which could then be used as an alternative to those derived from the ATNF catalogue, especially in the Extragalactic case. Moreover, the inclusion of angular distribution of the NSs would allow to perform a template-based matched-filtering search using the  $\lambda$ -statistics from Talukder et al. (2011), which

may set less conservative upper limits. Finally, from the synthesised population, the corresponding SGWB signal could be simulated, and its prospects for detection and characterisation could be examined within the networks of the future detector. Two ways of doing this would be to consider a network, where KAGRA and the future LIGO-India (Saleem et al. 2021) are included, or considering the next-generation interferometers, such as Einstein Telescope (Punturo et al. 2010) and Cosmic Explorer (Reitze et al. 2019), and evaluate their impact on these kinds of searches. These possibilities will be explored in future work.

## ACKNOWLEDGEMENTS

This material is based upon work supported by NSF’s LIGO Laboratory which is a major facility fully funded by the National Science Foundation. This research has used data obtained from the Gravitational Wave Open Science Center, a service of LIGO Laboratory, the LIGO Scientific Collaboration and the Virgo Collaboration. LIGO Laboratory and Advanced LIGO are funded by the United States National Science Foundation (NSF) as well as the Science and Technology Facilities Council (STFC) of the United Kingdom, the Max-Planck-Society (MPS), and the State of Niedersachsen/Germany for support of the construction of Advanced LIGO and construction and operation of the GEO600 detector. Additional support for Advanced LIGO was provided by the Australian Research Council. Virgo is funded, through the European Gravitational Observatory (EGO), by the French Centre National de Recherche Scientifique (CNRS), the Italian Istituto Nazionale della Fisica Nucleare (INFN) and the Dutch Nikhef, with contributions by institutions from Belgium, Germany, Greece, Hungary, Ireland, Japan, Monaco, Poland, Portugal, and Spain.

We acknowledge the use of Caltech LDAS clusters and the supercomputing facilities of the Université catholique de Louvain (CISM/UCL) and the Consortium des Équipements de Calcul Intensif en Fédération Wallonie Bruxelles (CÉCI), funded by the Fond de la Recherche Scientifique de Belgique (F.R.S.-FNRS) under convention 2.5020.11 and by the Walloon Region. The authors gratefully acknowledge the support of the NSF, STFC, INFN and CNRS for provision of computational resources.

The authors thank Patrick Meyers for carefully reading the manuscript and providing valuable comments. This work significantly benefited from the interactions with the Stochastic Working Group of the LIGO-Virgo-KAGRA Scientific Collaboration. We also thank T. Regimbau, D. Agarwal, Brendan T. Reed, Alex Deibel, and C. J. Horowitz for useful discussions.

F.D.L. is supported by a FRIA Grant of the Belgian Fund for Research, F.R.S.-FNRS. A.L.M. is a beneficiary of a FSR Incoming Postdoctoral Fellowship. This article has a LIGO document number LIGO-P2200050.

## DATA AVAILABILITY

This research has made use of data or software obtained from the Gravitational Wave Open Science Center ([gw-openscience.org](http://gw-openscience.org)) ([Abbott et al. 2021g](#)), a service of LIGO Laboratory, the LIGO Scientific Collaboration, the Virgo Collaboration, and KAGRA. Publicly available “Data for Upper Limits on the Isotropic Gravitational-Wave Background from Advanced LIGO’s and Advanced Virgo’s Third Observing Run” from [Abbott et al. \(2021e\)](#) has been used as well within the stochastic analysis.

## REFERENCES

- Aasi J., et al., 2013, *Phys. Rev. D*, 88, 102002
- Aasi J., et al., 2015, *CQGra*, 32, 074001
- Abbott R. e. a., 2021a, *Phys. Rev. D*, 104, 022004
- Abbott R. e. a., 2021b, *Phys. Rev. D*, 104, 022005
- Abbott B., et al., 2007, *Phys. Rev. D*, 76, 082003
- Abbott B. P., et al., 2017, *Astrophys. J. Lett.*, 851, L16
- Abbott B. P., et al., 2018, *Physical Review Letters*, 120, 091101
- Abbott B. P., et al., 2019, *The Astrophysical Journal*, 875, 160
- Abbott R., et al., 2020, *Astrophys. J. Lett.*, 902, L21
- Abbott R., et al., 2021f, All-sky, all-frequency directional search for persistent gravitational-waves from Advanced LIGO’s and Advanced Virgo’s first three observing runs ([arXiv:2110.09834](#))
- Abbott R., et al., 2021c, Constraints on dark photon dark matter using data from LIGO’s and Virgo’s third observing run ([arXiv:2105.13085](#))
- Abbott R., et al., 2021e, Data for Upper Limits on the Isotropic Gravitational-Wave Background from Advanced LIGO’s and Advanced Virgo’s Third Observing Run, <https://dcc.ligo.org/LIGO-G2001287/public>
- Abbott R., et al., 2021b, Narrowband searches for continuous and long-duration transient gravitational waves from known pulsars in the LIGO-Virgo third observing run ([arXiv:2112.10990](#))
- Abbott R., et al., 2021d, Search of the Early O3 LIGO Data for Continuous Gravitational Waves from the Cassiopeia A and Vela Jr. Supernova Remnants ([arXiv:2111.15116](#))
- Abbott R., et al., 2021a, Searches for Gravitational Waves from Known Pulsars at Two Harmonics in the Second and Third LIGO-Virgo Observing Runs ([arXiv:2111.13106](#))
- Abbott R., et al., 2021g, *SoftwareX*, 13, 100658
- Abbott R., et al., 2021h, *Phys. Rev. D*, 104, 082004
- Abbott R., et al., 2021i, *Astrophys. J.*, 913, L27
- Abbott R., et al., 2021j, *Astrophys. J.*, 921, 80
- Abbott R., et al., 2022, All-sky search for continuous gravitational waves from isolated neutron stars using Advanced LIGO and Advanced Virgo O3 data ([arXiv:2201.00697](#))
- Acernese F., et al., 2015, *CQGra*, 32, 024001
- Ade P. A. R., et al., 2016, *Astron. Astrophys.*, 594, A13
- Ain A., Dalvi P., Mitra S., 2015, *Phys. Rev. D*, 92, 022003
- Ain A., Suresh J., Mitra S., 2018, *Phys. Rev. D*, 98, 024001
- Akutsu T., et al., 2021, *PTEP*, 2021, 05A101
- Allen B., Ottewill A. C., 1997, *Phys. Rev. D*, 56, 545
- Allen B., Romano J. D., 1999, *Phys. Rev. D*, 59, 102001
- Ballmer S. W., 2006, *Classical and Quantum Gravity*, 23, S179
- Banagiri S., Sun L., Coughlin M. W., Melatos A., 2019, *Phys. Rev. D*, 100, 024034
- Bar-Kana R., 1994, *Phys. Rev. D*, 50, 1157
- Buono M., Rosa R. D., D’Onofrio L., Errico L., Palomba C., Piccinni O. J., Sequino V., 2021, *Classical and Quantum Gravity*, 38, 135021
- Christensen N., 1992, *Phys. Rev. D*, 46, 5250
- Cook J. L., Sorbo L., 2012, *Phys. Rev. D*, 85, 023534
- Cornish N. J., Romano J. D., 2015, *Phys. Rev. D*, 92, 042001
- Cusin G., Pitrou C., Uzan J.-P., 2017, *Phys. Rev. D*, 96, 103019
- Cusin G., Dvorkin I., Pitrou C., Uzan J.-P., 2018, *Phys. Rev. Lett.*, 120, 231101
- Cusin G., Durrer R., Ferreira P. G., 2019, *Phys. Rev. D*, 99, 023534
- Dergachev V., Papa M. A., Steltner B., Eggenstein H.-B., 2019, *Phys. Rev. D*, 99, 084048
- Dhurandhar S., Tagoshi H., Okada Y., Kanda N., Takahashi H., 2011, *Phys. Rev. D*, 84, 083007
- Diehl R., et al., 2006, *Nature*, 439, 45
- Dvorkin I., Uzan J.-P., Vangioni E., Silk J., 2016, *Phys. Rev. D*, 94, 103011
- Fan X., Chen Y., Messenger C., 2016, *Phys. Rev. D*, 94, 084029
- Flanagan E. E., 1993, *Phys. Rev. D*, 48, 2389
- Górski K. M., Hivon E., Banday A. J., Wandelt B. D., Hansen F. K., Reinecke M., Bartelman M., 2005, *Astrophys. J.*, 622, 759
- Guo H.-K., Riles K., Yang F.-W., Zhao Y., 2019, *Communications Physics*, 2, 1
- Haskell B., Patruno A., 2017, *Phys. Rev. Lett.*, 119, 161103
- Hughes S. A., 2014, *Physics of the Dark Universe*, 4, 86
- Inayoshi K., Kashiyama K., Visbal E., Haiman Z., 2021, *Astrophys. J.*, 919, 41
- Isi M., Sun L., Brito R., Melatos A., 2019, *Phys. Rev. D*, 99, 084042
- Jenkins A. C., Sakellariadou M., 2018, *Phys. Rev. D*, 98, 063509
- Jenkins A. C., Sakellariadou M., Regimbau T., Slezak E., 2018, *Phys. Rev. D*, 98, 063501
- Jones D. I., Andersson N., 2002, *Mon. Not. Roy. Astron. Soc.*, 331, 203
- Juliana P. O., 2022, Status and perspectives of Continuous Gravitational Wave searches ([arXiv:2202.01088](#))
- Kamionkowski M., Kosowsky A., Turner M. S., 1994, *Phys. Rev. D*, 49, 2837
- Kosowsky A., Turner M. S., Watkins R., 1992, *Phys. Rev. D*, 45, 4514
- Lasky P. D., 2015, *Publ. Astron. Soc. Austral.*, 32, e034
- Lasky P. D., Bennett M. F., Melatos A., 2013, *Phys. Rev. D*, 87, 063004
- Lorimer D. R., 2008, *Living Rev. Rel.*, 11, 8
- Lorimer D. R., 2012, *Proceedings of the International Astronomical Union*, 8, 237–242
- Lorimer D. R., et al., 2019, Radio Pulsar Populations ([arXiv:1903.06526](#))
- Maggiore M., 2007, *Gravitational Waves. Vol. 1: Theory and Experiments*
- Manchester R. N., Hobbs G. B., Teoh A., Hobbs M., 2005, *Astron. J.*, 129, 1993
- Marassi S., Schneider R., Corvino G., Ferrari V., Portegies Zwart S., 2011, *Phys. Rev. D*, 84, 124037
- Mazumder N., Mitra S., Dhurandhar S., 2014, *Phys. Rev. D*, 89, 084076
- Meadors G. D., Goetz E., Riles K., 2016, *Class. Quant. Grav.*, 33, 105017
- Miller A., Astone P., et al., 2018, *Phys. Rev. D*, 98, 102004
- Miller A. L., Astone P., et al., 2019, *Phys. Rev. D*, 100, 062005
- Miller A. L., Aggarwal N., Clesse S., De Lillo F., 2021a, Constraints on planetary and asteroid-mass primordial black holes from continuous gravitational-wave searches ([arXiv:2110.06188](#))
- Miller A. L., Clesse S., De Lillo F., Bruno G., Depasse A., Tanasijczuk A., 2021b, *Phys. Dark Univ.*, 32, 100836
- Miller A. L., et al., 2021c, *Phys. Rev. D*, 103, 103002
- Mingarelli C. M. F., Taylor S. R., Sathyaprakash B. S., Farr W. M., 2019, Understanding  $\Omega_{\text{gw}}(f)$  in Gravitational Wave Experiments ([arXiv:1911.09745](#))
- Mitra S., Dhurandhar S., Souradeep T., Lazzarini A., Mandic V., Bose S., Ballmer S., 2008, *Phys. Rev. D*, 77, 042002
- Mytidis A., Coughlin M., Whiting B., 2015, *The Astrophysical Journal*, 810, 27
- Mytidis A., Panagopoulos A. A., Panagopoulos O. P., Miller A., Whiting B., 2019, *Phys. Rev. D*, 99, 024024
- Okada Y., Kanda N., Dhurandhar S., Tagoshi H., Takahashi H., 2012, *J. Phys. Conf. Ser.*, 363, 012040
- Oliver M., Keitel D., Sintes A. M., 2019, *Phys. Rev. D*, 99, 104067
- Osborne E. L., Jones D. I., 2020, *Mon. Not. Roy. Astron. Soc.*, 494, 2839
- Owen B. J., Lindblom L., Cutler C., Schutz B. F., Vecchio A., Andersson N., 1998, *Phys. Rev. D*, 58, 084020
- Palomba C., et al., 2019, *Phys. Rev. Lett.*, 123, 171101
- Piccinni O. J., et al., 2020, *Phys. Rev. D*, 101, 082004
- Pierce A., Riles K., Zhao Y., 2018, *Phys. Rev. Lett.*, 121, 061102
- Pitkin M., Messenger C., Fan X., 2018, *Phys. Rev. D*, 98, 063001
- Punturo M., et al., 2010, *Class. Quant. Grav.*, 27, 194002
- Reed B. T., Deibel A., Horowitz C. J., 2021, *Astrophys. J.*, 921, 89
- Regimbau T., 2011, *Res. Astron. Astrophys.*, 11, 369



- Reitze D., et al., 2019, *Bulletin of the AAS*, 51  
 Riles K., 2017, *Mod. Phys. Lett. A*, 32, 1730035  
 Romano J. D., Cornish N. J., 2017, *Living Rev. Rel.*, 20, 2  
 Rosado P. A., 2011, *Phys. Rev. D*, 84, 084004  
 Rosado P. A., 2012, *Phys. Rev. D*, 86, 104007  
 Saleem M., et al., 2021, *Classical and Quantum Gravity*, 39, 025004  
 Sieniawska M., Beijger M., 2019, *Universe*, 5, 217  
 Singh N., Haskell B., Mukherjee D., Bulik T., 2020, *Mon. Not. Roy. Astron. Soc.*, 493, 3866  
 Story S. A., Gonthier P. L., Harding A. K., 2007, *The Astrophysical Journal*, 671, 713  
 Sun L., Melatos A., 2019, *Phys. Rev. D*, 99, 123003  
 Sun L., Brito R., Isi M., 2020, *Phys. Rev. D*, 101, 063020  
 Suresh J., Ain A., Mitra S., 2021, *Phys. Rev. D*, 103, 083024  
 Talukder D., Mitra S., Bose S., 2011, *Phys. Rev. D*, 83, 063002  
 Talukder D., Thrane E., Bose S., Regimbau T., 2014, *Phys. Rev. D*, 89, 123008  
 Tenorio R., Keitel D., Sintés A. M., 2021, *Universe*, 7, 474  
 Thrane E., Romano J. D., 2013, *Phys. Rev. D*, 88, 124032  
 Thrane E., Ballmer S., Romano J. D., Mitra S., Talukder D., Bose S., Mandic V., 2009, *Phys. Rev. D*, 80, 122002  
 Turner M. S., 1997, *Phys. Rev. D*, 55, R435  
 Ushomirsky G., Cutler C., Bildsten L., 2000, *Mon. Not. Roy. Astron. Soc.*, 319, 902  
 Virtanen P., et al., 2020, *Nature Methods*, 17, 261  
 Watanabe Y., Komatsu E., 2006, *Phys. Rev. D*, 73, 123515  
 Wu C.-J., Mandic V., Regimbau T., 2013, *Phys. Rev. D*, 87, 042002  
 Zhu X.-J., Howell E., Regimbau T., Blair D., Zhu Z.-H., 2011, *Astrophys. J.*, 739, 86  
 Zhu X.-J., Howell E. J., Blair D. G., Zhu Z.-H., 2013, *Mon. Not. Roy. Astron. Soc.*, 431, 882  
 Zonca A., Singer L. P., Lenz D., Reinecke M., Rosset C., Hivon E., Gorski K. M., 2019, *Journal of Open Source Software*, 4, 1298

## APPENDIX A: DERIVATION OF THE SPECTRAL SHAPE

Here, we present a heuristic procedure to get the expression of the spectral shape  $H(f)$  in equation (2). It is known that the GW power emitted by a pulsar at a given frequency can be expressed as (Maggiore 2007):

$$P(f) = \frac{32\pi^6 G}{5c^5} \varepsilon^2 I_{zz}^2 f^6, \quad (\text{A1})$$

and is linked to the GW energy density at a distance  $d$  from the source through the relation

$$\rho_{\text{gw}}(f) = \frac{P(f)}{4\pi c d^2}. \quad (\text{A2})$$

Now, let us consider a population of NSs, each one emitting GW at a frequency  $f_j$  and from the direction  $\hat{n}_j$ , where  $j = 1, 2, \dots, N_0$  and  $N_0$  is the total number of pulsars. Then, the corresponding GW energy density ratio can be expressed as

$$\begin{aligned} \Omega_{\text{gw}}(f, \hat{n}) &= \frac{f}{\rho_c} \sum_{j=1}^{N_0} \frac{P_j}{4\pi c d_j^2} \delta(f - f_j) \delta^2(\hat{n}, \hat{n}_j) \\ &= \frac{f \langle P \rangle_{\text{NS}}}{4\pi \rho_c c} \left\langle \frac{1}{d^2} \right\rangle_{\text{NS}} N_0 \Psi(f, \hat{n}), \end{aligned} \quad (\text{A3})$$

where  $\Psi(f, \hat{n})$  is the frequency-angular distribution of the NS population. We take the ensemble average over pulsars parameters in the second line of above equation. Finally, plugging equation (A1) in equation (A3) and using the definition of spectral shape (equation

(17)), we get

$$\begin{aligned} H(f) &= \frac{3H_0^2}{2\pi^2 f^3} \int d^2 \hat{n} \Omega_{\text{gw}}(f, \hat{n}) \\ &= \frac{32\pi^4 G^2 \langle \varepsilon^2 \rangle_{\text{NS}} \langle I_{zz}^2 \rangle_{\text{NS}}}{5c^8 \langle d^2 \rangle_{\text{NS}}} f^4 \Phi(f) N_0, \end{aligned} \quad (\text{A4})$$

this is identical to equation (2) where  $\Phi(f) \equiv \int d^2 \Omega_{\hat{n}} \Psi(f, \hat{n})$ .

## APPENDIX B: THE ELLIPTICITY ESTIMATOR UNCERTAINTY: GENERAL CASE

Here, we derive the expression of the variance  $\sigma_{\hat{\varepsilon}}^2(f_k)$  of the estimator of the average ellipticity  $\hat{\varepsilon}_{\text{av}}(f_k)$  in the general case, where  $\hat{\varepsilon}_{\text{av}}(f_k) > 0$ . The procedure is not complex conceptually: it is necessary to evaluate the first and second-order expectation values starting from the likelihood in equation (22) and combine them to get  $\sigma_{\hat{\varepsilon}}^2(f_k)$ , but some algebra is required.

From the expressions (where  $D_\nu(z)$  is a parabolic cylinder function and we omit the frequency label in the last expression)

$$\begin{aligned} \langle \varepsilon_{\text{av}}(f_k) \rangle &\equiv \int_0^\infty p_\varepsilon(\hat{\varepsilon}_{\text{av}}(f_k) | \varepsilon_{\text{av}}(f_k)) \varepsilon_{\text{av}} d\varepsilon_{\text{av}} \\ &= \sqrt{\frac{\sigma_{\hat{\Omega}}}{2\xi}} D_{-3/2} \left( -\frac{\hat{\varepsilon}_{\text{av}}^2 \xi}{\sigma_{\hat{\Omega}}} \right) \exp \left[ -\frac{\hat{\varepsilon}_{\text{av}}^4 \xi^2}{4\sigma_{\hat{\Omega}}^2} \right] \end{aligned} \quad (\text{B1})$$

and

$$\begin{aligned} \langle \varepsilon_{\text{av}}^2(f_k) \rangle &\equiv \int_0^\infty p_\varepsilon(\hat{\varepsilon}_{\text{av}}(f_k) | \varepsilon_{\text{av}}(f_k)) \varepsilon_{\text{av}}^2 d\varepsilon_{\text{av}} \\ &= \sqrt{\frac{2}{\pi}} \frac{\sigma_{\hat{\Omega}}}{\xi} D_{-2} \left( -\frac{\hat{\varepsilon}_{\text{av}}^2 \xi}{\sigma_{\hat{\Omega}}} \right) \exp \left[ -\frac{\hat{\varepsilon}_{\text{av}}^4 \xi^2}{4\sigma_{\hat{\Omega}}^2} \right], \end{aligned} \quad (\text{B2})$$

it is straightforward to show

$$\begin{aligned} \sigma_{\hat{\varepsilon}}^2(f_k) &= \langle \varepsilon_{\text{av}}^2(f_k) \rangle - \langle \varepsilon_{\text{av}}(f_k) \rangle^2 \\ &= \sqrt{\frac{2}{\pi}} \frac{\sigma_{\hat{\Omega}}}{\xi} D_{-2} \left( -\frac{\hat{\varepsilon}_{\text{av}}^2 \xi}{\sigma_{\hat{\Omega}}} \right) \exp \left[ -\frac{\hat{\varepsilon}_{\text{av}}^4 \xi^2}{4\sigma_{\hat{\Omega}}^2} \right] - \\ &\quad - \frac{1}{2} \frac{\sigma_{\hat{\Omega}}}{\xi} D_{-3/2}^2 \left( -\frac{\hat{\varepsilon}_{\text{av}}^2 \xi}{\sigma_{\hat{\Omega}}} \right) \exp \left[ -\frac{\hat{\varepsilon}_{\text{av}}^4 \xi^2}{2\sigma_{\hat{\Omega}}^2} \right]. \end{aligned} \quad (\text{B3})$$

The limit  $\varepsilon \ll 1$  in equation (23) is recovered by observing and using

$$D_\nu(z) |_{z \ll 1} \approx \frac{2^{-(\nu+2)/2} \Gamma(-\frac{\nu}{2})}{\Gamma(-\nu)}, \quad (\text{B4})$$

where  $\Gamma(z)$  is Euler's Gamma function.

## APPENDIX C: SEARCH FOR SGWB FROM NS HOTPOTS

Here, we present how we have derived the limits on  $\Omega_{\text{gw}}^{\text{patch}}(f)$  of a patch in the sky to use as input in section 4.2 to get the constraints on the average ellipticity of the NS hotspots.

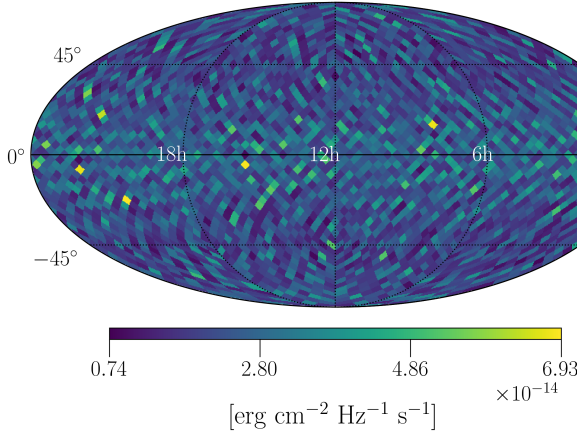


**Figure C1.** Upper limit sky maps on GW energy flux from the broadband-radiometer analysis for the model  $\bar{H}(f)$  in equation (C8). Here the NSs frequency distribution  $\Phi(f)$  is the one built from the ATNF catalogue as described in section 2. The sky map is represented as a color bar plot on a Mollweide projection of the sky in ecliptic coordinates with  $N_{\text{side}} = 16$ .

### C1 The directional radiometer search

The directional radiometer search drops the assumption of the SGWB being isotropic (Jenkins & Sakellariadou 2018; Mazumder et al. 2014; Cusin et al. 2018; Jenkins et al. 2018; Rosado 2012; Wu et al. 2013; Lasky et al. 2013; Cusin et al. 2017). This means that the background cannot be simply characterised by considering  $\Omega_{\text{gw}}(f)$  in equation (6), but rather the frequency-angular dependent density parameter  $\Omega_{\text{gw}}(f, \hat{n})$  (measured in  $\text{sr}^{-1}$ ):

$$\Omega_{\text{gw}}(f, \hat{n}) = \frac{f}{\rho_c} \frac{d^3 \rho_{\text{gw}}(f, \hat{n})}{df d^2 \hat{n}} = \frac{2\pi^2}{3H_0^2} f^3 \mathcal{P}(f, \hat{n}), \quad (\text{C1})$$

with  $\mathcal{P}(f, \hat{n})$  being the GW strain power.

To measure the anisotropies, the radiometer search introduces a maximum-likelihood (ML) estimator (Mitra et al. 2008; Thrane et al. 2009), as statistic, at each frequency and each direction (Abbott et al. 2021f)  $\hat{\mathcal{P}}(f, \hat{n})$  with cross-correlation matrix  $\sigma_{\hat{n}, \hat{n}'}(f)$ :

$$\hat{\mathcal{P}}(f, \hat{n}) = \sum_{\hat{n}'} [\Gamma_{\hat{n}\hat{n}'}(f)]^{-1} X_{\hat{n}'}(f), \quad (\text{C2})$$

$$\sigma_{\hat{n}, \hat{n}'}(f) = [\Gamma_{\hat{n}\hat{n}'}(f)]^{-1/2}, \quad (\text{C3})$$

where  $X_{\hat{n}'}(f)$  is called “dirty map” and  $\Gamma_{\hat{n}\hat{n}'}$  is the Fisher information matrix in the small-signal limit. The summation over  $\hat{n}'$  implies integration over the solid angle. The dirty map represents the sky seen through the response of a set of independent baselines  $IJ$ , defined as

$$X_{\hat{n}}(f) = \tau \Delta f \Re \sum_{IJ, I'} \frac{[\gamma_{IJ}(t; f)]_{\hat{n}}^* \hat{C}_{IJ}(t; f)}{P_I(t; f) P_J(t; f)}, \quad (\text{C4})$$

where  $\hat{C}_{IJ}(t; f) \equiv (2/\tau) \bar{s}_I^*(t; f) \bar{s}_J(t; f)$  is the cross-correlation spectral density, while  $\gamma_{IJ}(t; f, \hat{n})$  is the directional overlap reduction function, which is proportional to the isotropic one in equation (8) when integrated over the sky. The Fisher information matrix encodes the uncertainty in the measurement of the dirty map, and is defined as

$$\Gamma_{\hat{n}, \hat{n}'}(f) = \tau \Delta f \Re \sum_{IJ, I'} \frac{[\gamma_{IJ}(t; f)]_{\hat{n}}^* [\gamma_{IJ}(t; f)]_{\hat{n}'}}{P_I(t; f) P_J(t; f)}. \quad (\text{C5})$$

The ML estimator  $\hat{\mathcal{P}}(f, \hat{n})$  in equation (C2), involves the inversion of  $\Gamma_{\hat{n}, \hat{n}'}(f)$ , which can be singular in general and must be regularised. However, for point-like sources considered here, we can work by employing the pixel basis

$$\mathcal{P}(f, \hat{n}) \equiv \mathcal{P}(f, \hat{n}') \delta^2(\hat{n}, \hat{n}'), \quad (\text{C6})$$

and ignore the correlation among neighbourhood directions in the sky (Abbott 2021b; Abbott et al. 2021f), and the Fisher information matrix is no longer singular and becomes diagonal. With this caveat, the estimator can be used to set upper limits on  $\Omega_{\text{gw}}(f, \hat{n})$  and related quantities.

### C2 SGWB from NS hotspots in the sky

To specialise the framework to our search for a SGWB from NS hotspots, we make the following, standard, ansatz about the factorisability of  $\hat{\mathcal{P}}(f, \hat{n})$  in a frequency and direction dependent only terms:

$$\mathcal{P}(f, \hat{n}) = \bar{H}(f) \mathcal{P}(\hat{n}), \quad (\text{C7})$$

where  $\bar{H}(f)$  is defined in such a way that  $\bar{H}(f_{\text{ref}}) = 1$ ,  $\mathcal{P}(\hat{n})$  is the angular distribution of gravitational-wave power to be estimated by the search. For the signal model presented in section 3,  $\bar{H}(f)$  turns out to be

$$\bar{H}(f) = \left( \frac{f}{f_{\text{ref}}} \right)^4 \frac{\Phi(f)}{\Phi(f_{\text{ref}})}. \quad (\text{C8})$$

Using the above formalism, it is possible to integrate  $\hat{\mathcal{P}}(f, \hat{n})$  (or, equivalently  $\hat{\Omega}_{\text{gw}}(f, \hat{n})$ ) over the frequencies, to get a set of broadband estimators  $\hat{\mathcal{P}}_{\text{ref}}(\hat{n})$ , or over the sky directions of a sky patch, to get a set of narrowband estimators  $\hat{\mathcal{P}}_{\text{ref}}^{\text{patch}}(f_k)$ , or even both frequencies and direction, getting a broadband estimator of the SGWB of a sky patch  $\hat{\mathcal{P}}_{\text{ref}}^{\text{patch}}$ . The master formulas for the integrated estimator over a set of frequencies and directions, and the relative uncertainty, is given by

$$\hat{\mathcal{P}}_{\text{ref}}^{\text{patch}} = \frac{\sum_{k,j} \hat{\mathcal{P}}(f_k, \hat{n}_j) \sigma^{-2}(f_k, \hat{n}_j) \bar{H}(f)}{\sum_{k,j} \sigma^{-2}(f_k, \hat{n}_j) \bar{H}(f)^2}, \quad (\text{C9})$$

$$\sigma_{\text{ref}}^{\text{patch}} = \left( \sum_{k,j} \sigma^{-2}(f_k, \hat{n}_j) \bar{H}(f)^2 \right)^{-1/2}. \quad (\text{C10})$$

Within this framework, we derive the following quantities: a broadband estimator for each sky direction  $\hat{\mathcal{P}}_{\text{ref}}^{\text{sky}}(\hat{n})$ , a set of narrowband estimators for each patch  $\hat{\mathcal{P}}_{\text{ref}}^{\text{patch}}(f_k)$ , and a broadband estimator for each patch  $\hat{\mathcal{P}}_{\text{ref}}^{\text{patch}}$ . The broadband estimators are evaluated to get information about the SGWB from a NS population, when one allows for an unknown spatial distribution of the population, compared to the isotropic case. These estimators are translated into estimators of the GW energy flux, given the astrophysical nature of the source,

$$\hat{\mathcal{F}}_{\text{ref}}(\hat{n}) = \frac{c^3 \pi}{4G} f_{\text{ref}}^2 \hat{\mathcal{P}}_{\text{ref}}(\hat{n}), \quad (\text{C11})$$

at a reference frequency  $f_{\text{ref}}$ , from which the relative UL are calculated and illustrated in figure C1. The narrowband estimators for every patch, instead, are converted to narrowband estimators of the density parameter  $\hat{\Omega}_{\text{gw}}^{\text{patch}}(f_k)$  by means of equation (C1), and are used as input for the evaluation of constraints on the average ellipticity of the different NS populations in section 4.2.

This paper has been typeset from a  $\text{\TeX}/\text{\LaTeX}$  file prepared by the author.